http://dx.doi.org/10.5012/bkcs.2012.33.6.1851

Enhanced Gas Sensing Properties of Pt-Loaded TeO_2 Nanorods

Changhyun Jin, Sunghoon Park, Hyunsu Kim, and Chongmu Lee*

Department of Materials science and Engineering, Inha University, Incheon 402-751, Korea
**E-mail: cmlee@inha.ac.kr*
Received December 21, 2011, Accepted February 28, 2012

The NO_2 gas sensing properties of multiple-networked, Pt-loaded TeO_2 nanorod sensors were examined. Scanning electron microscopy revealed nanowires with diameters of 50-100 nm and lengths of a few micrometers. Transmission electron microscopy and X-ray diffraction showed that the nanrods were tetragonal-structured, single crystal TeO_2. The Pt-loaded TeO_2 nanorod sensors exhibited sensitivities of 11.00, 10.26, 11.23 and 11.97% at NO_2 concentrations of 10, 50, 100 and 200 ppm, respectively, at 300 °C. These sensitivities were more than 10 times higher than those of bare-TeO_2 nanorod sensors. The response times of the sensors were 310, 260, 270 and 230 sec at NO_2 concentrations of 10, 50, 100 and 200 ppm, respectively. The recovery times of the Pt-loaded TeO_2 nanorods were 390, 330, 335, and 330 sec at NO_2 concentrations of 10, 50, 100 and 200 ppm, respectively. The origin of the enhanced sensing properties of the TeO_2 nanorods by Pt loading is discussed.

Key Words : Nanorods, TeO_2, Pt-doping, Gas sensor, NO_2

Introduction

One-dimensional (1D) nanostructure-based metal oxide sensors have attracted considerable attention because of their higher sensitivity, superior spatial resolution and rapid response due to the high surface-to-volume ratios than thin film-type gas sensors.[1-5] On the other hand, they have several problems to overcome, such as a lack of sensitivity and very low sensitivity to low gas concentrations at room temperature. The development of highly selective and controllably-sensitized devices remains a challenge.

Tellurium dioxide (TeO_2) is an attractive semiconductor oxide material with unique physical and chemical properties suitable for a wide range of technological applications, such as deflectors,[1] modulators,[2] dosimeters,[3,4] optical storage material,[5] laser devices[6] and gas sensors.[7,8] TeO_2 nanorods have been synthesized by the thermal evaporation of Te powders,[9] laser ablation of Te,[7] and direct thermal oxidation of Te at ambient pressure in a flow of O_2 without the presence of a catalyst.[10] Microcrystals of TeO_2 have been synthesized by the hydrolysis of tellurium isopropoxide in the presence of a tetra alkyl ammonium bromide solution.[11]

Regarding TeO_2 nanostructure sensors, the gas sensing properties of the TeO_2 nanowires synthesized by the thermal evaporation of Te metal in air were reported for the first time.[12] Their report demonstrated the possibility of making low power consumption gas sensors sensitive to toxic gases, such as NO_2, NH_3 and H_2S using TeO_2 nanowires. Several techniques have been developed to enhance the sensitivity, selectivity, or lower the operational temperature of 1D nanostructure sensors. These include surface functionalization,[13-15] doping,[16-18] and heterostructure formation.[19-21] On the other hand, there are few reports on the application of these techniques to TeO_2 1D nanostructure sensors. This study examined the effect of Pt-doping on the NO_2 gas sensing properties of networked TeO_2 nanorods.

Experimental

TeO_2 nanorods were synthesized on p-type Si (100) substrates in a quartz tube furnace by the thermal evaporation of Te powders at 400 °C in air without the use of metal catalysts. Thermal evaporation was carried out for 1 h and the furnace was cooled to room temperature. The weight of the TeO_2 nanorods dispersed on a substrate was approximately 0.5 mg and the area of the sensing element was 7 mm × 10 mm. For platinum doping, a 40-μL ethanolic solution of platinic chloride ($H_2PtCl_6 \cdot 6H_2O$) at a concentration of 1.25×10^{-3} mol/L was poured onto the TeO_2 nanorod sensors. After annealing at 350 °C for 30 min under a flow of Ar gas (100 standard cubic centimeters per min (sccm)), two different types of gas sensors were fabricated: undoped and 2 wt % Pt-loaded TeO_2 nanorod sensors. The Pt concentration in the Pt-doped sensors was estimated by calculating the weight ratio of Pt in the ethanol solution of platinic chloride to the TeO_2 nanorods. The collected nanorod samples were characterized by scanning electron microscopy (SEM, Hitachi S-4200) equipped with an energy dispersive X-ray spectrometer (EDXS), transmission electron microscopy (TEM, Philips CM-200) and X-ray diffraction (XRD, Philips X'pert MRD diffractometer),

For the sensing measurements, Ni (~200 nm in thickness) and Au (~50 nm) thin films were deposited sequentially by sputtering to form electrodes with ohmic contact using an interdigital electrode mask. Figure 1 shows a schematic diagram of the multiple-networked TeO_2 nanorod sensors. The electrical and gas sensing properties of the bare and Pt-loaded TeO_2 nanorods were measured at room temperature

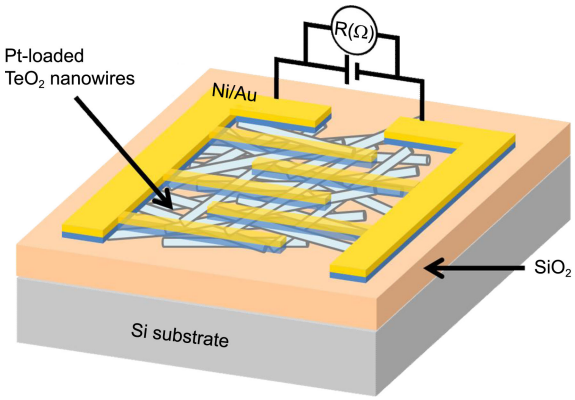

Figure 1. Schematic diagram of a multiple networked Pt-loaded TeO_2 nanorod sensor.

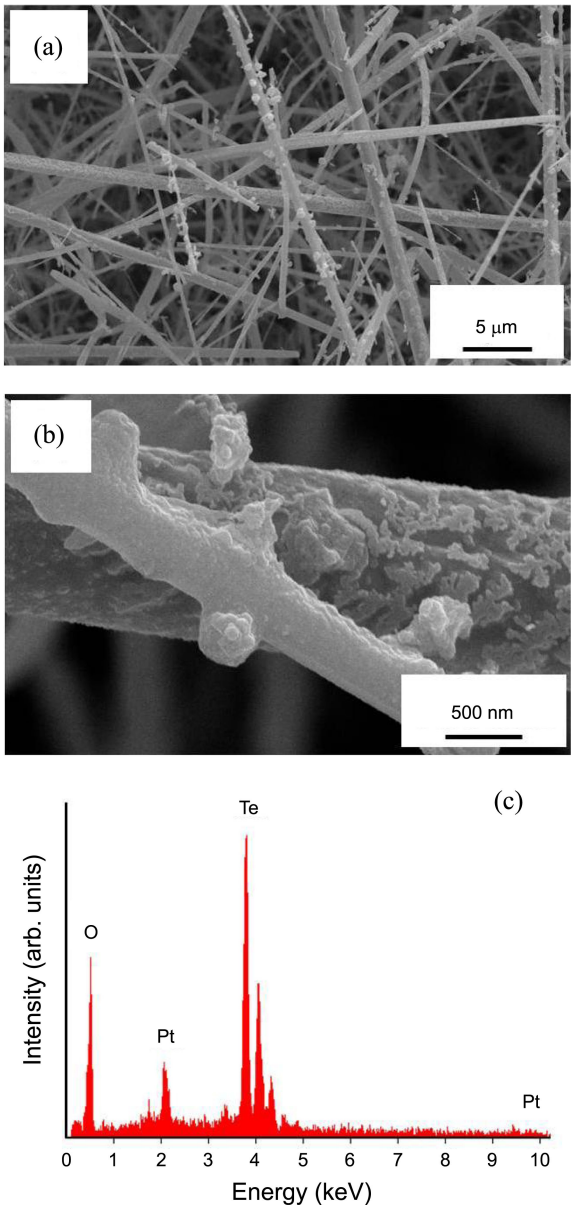

Figure 2. (a) SEM image of the Pt-loaded TeO_2 nanorods, Inset, enlarged SEM image of a typical TeO_2 nanowires. (b) Enlarged SEM image and (c) EDX spectrum of Pt-loaded TeO_2 nanorods.

using a home-made gas sensing measurement system. During the measurements, the nanorod gas sensors were placed in a sealed quartz tube with an electrical feed through. A given amount of NO_2 (> 99.99%) gas was injected into the testing tube through a microsyringe to obtain the given NO_2 concentration and the electrical resistance of the nanowires was monitored at the same time. The sensitivity of the p-type TeO_2 nanorod sensors was defined as $(R_a\text{-}R_g)/R_g$ for oxidizing gas NO_2, where R_a and R_g are the electrical resistances of the sensors in air and target gas, respectively. The response time is defined as the time needed for the change in electrical resistance to reach 90% of the equilibrium value after injecting the gas. The recovery time is defined as the time needed for the sensor to return to 90% above the original resistance in air after removing the gas.

Results and Discussion

Figure 2(a) shows FESEM images of the Pt-loaded TeO_2 nanorods prepared by the thermal evaporation of Te powders in air followed by Pt loading. Scanning electron microscopy revealed Pt-loaded TeO_2 nanorods with diameters of a few hundreds of nanometers and lengths of a few tens of micrometers. An enlarged SEM image (Fig. 2(b)) showed that the some of the Pt into the nanorods had precipitated as particles on the surface of the TeO_2 nanorods during the annealing process. Therefore, it might be a more appropriate to say that the surfaces of the TeO_2 nanorods are functionalized with Pt and the nanorods are loaded with Pt. EDX analysis of the nanorod (Fig. 2(c)) provided some evidence of Pt loading of TeO_2 nanorods.

Figure 3 shows a XRD pattern of the as-synthesized Pt-loaded TeO_2 nanorods. The main diffraction peaks in the pattern of the as-synthesized nanorods (Fig. 3) were indexed to a tetragonal structured, single crystal TeO_2, indicating that the nanomaterial is TeO_2. In addition to the reflections from TeO_2, two small sharp reflection peaks from Pt were identified. The low-magnification TEM image shows a typical Pt-loaded TeO_2 nanorod with a thickness of approximately 120 nm (Fig. 4(a)). Pt particles were distributed randomly over

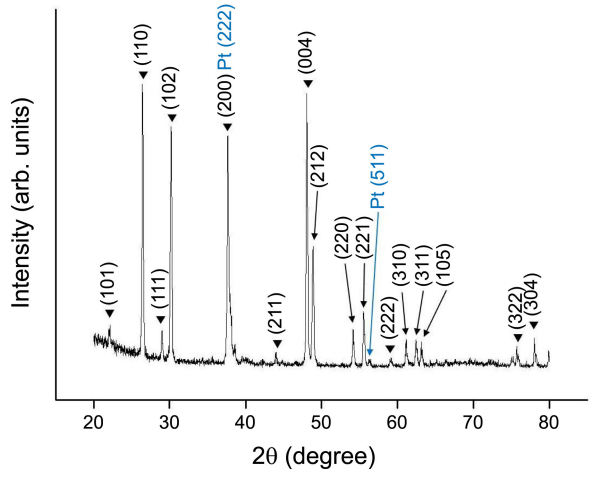

Figure 3. XRD pattern of the Pt-loaded TeO_2 nanorods.

the surface of the TeO_2 nanorod. The HRTEM image of the interfacial region of the Pt-particle and TeO_2 nanorod (Fig. 4(b)) revealed a Pt particle size of approximately 20 nm. The resolved spacing between the two neighboring parallel fringes in the particle and nanorod were approximately 0.22 and 0.24 nm, respectively, which are in good agreement with the interplanar spacings of the (111) plane of face-centered cubic-structured Pt (JCPDS No. 01-1190, a = 0.3912 nm) and the (200) plane of simple tetragonal-structured TeO_2 (JCPDS No. 78-1713, a = 0.481 nm and c = 0.7613 nm), respectively. The corresponding selected area electron diffraction (SAED) patterns recorded perpendicular to the long axis (Fig. 4(c)) that were indexed to the [20$\bar{1}$] zone axis of TeO_2. Two sets of spotty diffraction patterns were observed: a set of strong reflection spots and another set of dim ones. The strong reflection spots in the corre-

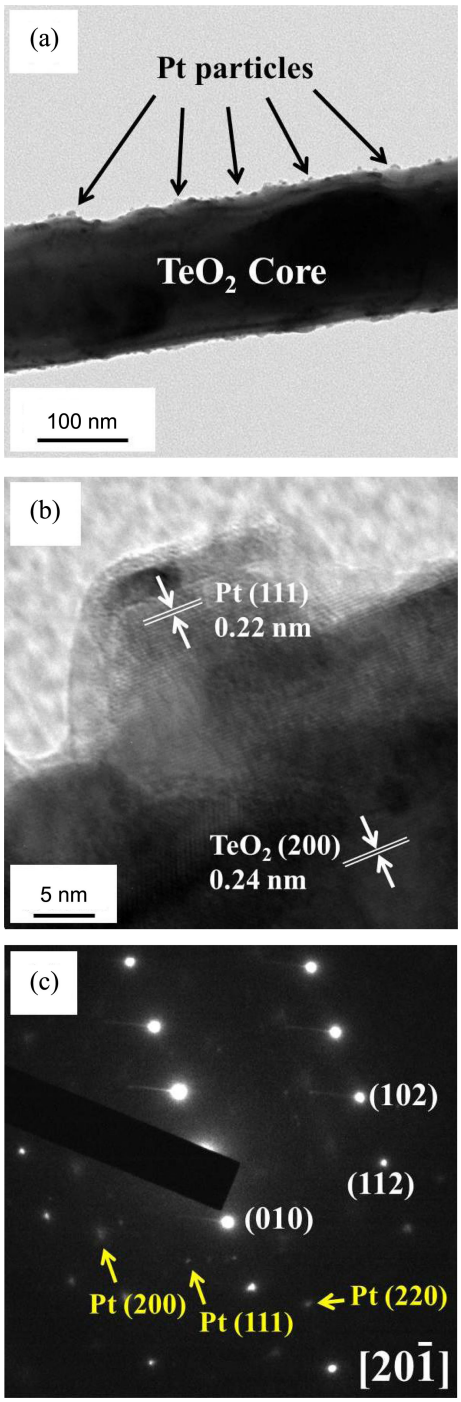

Figure 4. (a) Low-magnification TEM image of a typical Pt-loaded TeO_2 nanorod and (b) HRTEM image of a typical Pt-loaded TeO_2 nanorod at the TeO_2-Pt interface region. (c) corresponding SAED pattern.

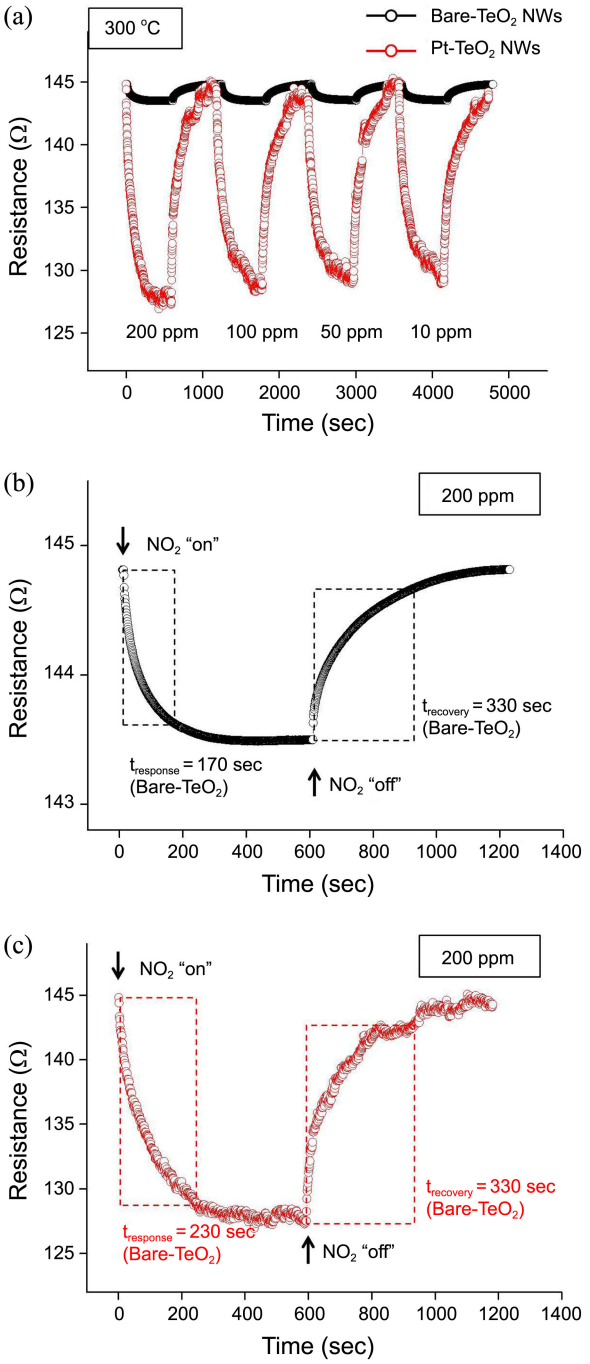

Figure 5. (a) Dynamic responses of the bare- and Pt-loaded TeO_2 nanorod sensors to NO_2 gas at 300 °C. (b) Enlarged part of the dynamic response of the bare-TeO_2 nanorod sensor in (a) at a NO_2 gas concentration of 200 ppm. (c) Enlarged part of the dynamic response of the Pt-loaded TeO_2 nanorod sensor in (a) at a NO_2 gas concentration of 200 ppm.

Table 1. Relative sensitivity measured at different NO_2 concentrations, for bare and Pt-loaded TeO_2 nanorod sensors

	Sensitivity (%)		Response time (sec)		Recovery time (sec)	
NO_2 Conc.	Bare-TeO_2	Pt-TeO_2	Bare-TeO_2	Pt-TeO_2	Bare-TeO_2	Pt-TeO_2
200 ppm	0.92	11.97	170	230	330	330
100 ppm	0.92	11.23	185	270	340	335
50 ppm	0.90	11.12	200	260	280	330
10 ppm	0.88	11.00	200	310	280	390

sponding selected area electron diffraction (SAED) pattern (Fig. 4(c)) were assigned to the (010), (102), and (112) reflections from tetragonal TeO_2 with the lattice constants, indicating that the TeO_2 nanorod in the TEM image is a single crystal. In addition to the reflections from TeO_2, several dim spots indexed to the (111), (200) and (220) reflections from face-centered cubic structured Pt were observed.

Figure 5(a) shows the dynamic sensing characteristics of multiple-networked bare- and Pt-doped TeO_2 nanorods to an oxidizing gas (NO_2) at room temperature. Figure 5(b) presents an enlarged part of Figure 5(a) at a NO_2 concentration of 200 ppm to highlight the moments of gas input and gas stop. The resistance responded well to NO_2 gas. The resistance decreased rapidly when the nanorod sensors were exposed to NO_2 gas and recovered completely to the initial value when the NO_2 gas supply was stopped and air was introduced. The nanorod sensors showed stable and reproducible responses for repeated testing cycles. Table 1 lists the sensitivities calculated from Figure 5(a). The Pt-loaded TeO_2 nanorods showed sensitivities of 11.00, 11.12, 11.23, and 11.97% at room temperature at NO_2 concentrations of 10, 50, 100 and 200 ppm, respectively (Table 1). The response times of the Pt-loaded TeO_2 nanorods were 310, 260, 270 and 230 sec at NO_2 concentrations of 10, 50,100 and 200 ppm, respectively. The recovery times of the Pt-loaded TeO_2 nanorods were 390, 330, 335 and 330 sec at NO_2 concentrations of 10, 50,100 and 200 ppm, respectively. These results highlight the potential use of Pt-loaded TeO_2 nanorods as a sensor for NO_2 gas detection. The NO_2 gas sensitivies of the Pt-loaded TeO_2 nanorods were comparable to those of other material sensors reported previously: ZnO nanorods (40% at 100 ppb NO_2),[22] SnO_2 nanobelts (230% at 300 ppb NO_2),[23] In_2O_3 nanowires (35% at 500 ppb NO_2),[24] WO_3 nanorods (30-200% at 1 ppm NO_2),[25] and SnO_2-core/ZnO-shell nanofibers (10-40%).[26]

The NO_2 gas sensing mechanism of the Pt-loaded TeO_2 nanorods can be explained based on the models proposed for the spill-over mechanism and metal catalyst-enhanced gas sensing of nanomaterials.[27] At lower temperatures, bulk defects equilibrate quite slowly because surface conduction is dominant. Surface conduction depends only on chemical sensitization. NO_2 is a strong oxidizing gas. After the TeO_2 nanorods are exposed to NO_2 gas, NO_2 molecules are adsorbed on the TeO_2 surface, which trap the lone-pair electrons of the dangling bond on the TeO_2 surface.[28] This results in the formation of a free hole, as shown in the following equations:

$$NO_{2(g)} \rightarrow NO_2^-{}_{(ad)} + h^+ \quad (1)$$

The holes combine with the electrons released from the surface reaction on the material, resulting in a decrease in electrical resistance. In the case of Pt-loaded TeO_2 nanorods, the adsorption of NO_2 gas and the formation of free holes by NO_2 gas were enhanced on the Pt nanoparticle surface because of the following two reasons:

(1) The TeO_2 nanorod surface is enriched with chemisorbed oxygen species due to the presence of the Pt clusters and the NO_2 gas is spilt over the TeO_2 nanorod surface by the Pt nanoparticles, so that one observes the enhanced sensing effect.

(2) As indicated by SEM (Fig. 2(b)) and TEM (Fig. 3(a)), the Pt nanoparticles have a larger surface to volume ratio than the TeO_2 nanorods owing to their particle-like shape and very irregular surface morphology as well as the high catalytic or conductive nature of Pt, which can lead to the enhanced adsorption of NO_2 gas. NO_2 molecules dissociate on catalytic Pt particles and then diffuse to the substrate, probably across and/or through the particles, where NO_2 molecules can interact with semiconducting TeO_2 nanorods to increase the conductance.[29] Therefore, NO_2 molecules dissociate and generate chemisorbed oxygen species much more rapidly due to the enhanced interaction by Pt.[30]

Consequently, the number of holes released from the gas species increases. In short, combination of the spillover effect and the enhancement of chemisorption and dissociation of gas enhances the electrical response of the Pt-loaded TeO_2 nanorod sensor to NO_2 gas.

Conclusions

Multiple-networked Pt-loaded TeO_2 nanorod sensors exhibited sensitivities more than 10 times higher than those of bare-TeO_2 nanorod sensors. The response and recovery times of Pt-loaded TeO_2 nanorods were somewhat longer than those of bare-TeO_2 nanorod sensors, but less than 7 min. These results are comparable to the NO_2 gas sensing data of other material sensors reported. The TeO_2 nanorod surface is enriched with chemisorbed oxygen species due to the presence of the Pt clusters and the NO_2 gas is spilt over the TeO_2 nanorod surface by the Pt nanoparticles, so that one observes the enhanced sensing effect. Another possible explanation is that the Pt nanoparticles have a larger surface to volume ratio than the TeO_2 nanorods owing to their

particle-like shape and very irregular surface morphology as well as the high catalytic or conductive nature of Pt, which can lead to the enhanced adsorption of NO_2 gas. NO_2 molecules dissociate on catalytic Pt particles and then diffuse to the substrate, probably across and/or through the particles, where NO_2 molecules can interact with semiconducting TeO_2 nanorods to increase the conductance. Therefore, NO_2 molecules dissociate and generate chemisorbed oxygen species much more rapidly due to the enhanced interaction by Pt. In short, the enhanced chemisorption of NO_2 gas molecules and the formation of holes by them enhances the electrical response of the Pt-loaded TeO_2 nanorod sensor to NO_2 gas.

Acknowledgments. This study was supported by the 2010 Core Research Program through the National Research Foundation of Korea (NRF) funded by the Ministry of Education, Science and Technology.

References

1. Warner, A. W.; White, D. L.; Bonner, W. A. *J. Appl. Phys.* **1972**, *43*, 4489.
2. Antonov, S. N. *Tech. Phys.* **2004**, *49*, 1329.
3. Arshak, K.; Korostynska, O. *Mater. Sci. Eng. B* **2004**, *107*, 224.
4. Arshak, K.; Korostynska, O. *Sensors* **2002**, *2*, 347.
5. Hodgson, S. N. B.; Weng, L. *J. Sol-Gel Sci. Technol.* **2000**, *18*, 145.
6. Hodgson, S. N. B.; Weng, L. *J. Mater. Sci.: Mater. Electron.* **2006**, *17*, 723.
7. Liu, Z.; Yamaznki, T.; Shen, Y.; Kikuta, T.; Nakatani, N. *Jpn. J. Appl. Phys.* **2008**, *47*, 771.
8. Liu, Z.; Yamaznki, T.; Shen, Y.; Kikuta, T.; Nakatani, N.; Kawabata, T. *Appl. Phys. Lett.* **2007**, *90*, 173119.
9. Jiang, Z.-Y.; Xie, Z.-X.; Zhang, X.-H.; Xie, S.-Y.; Huang, R.-B.; Zheng, L.-S. *Inorg. Chem. Commun.* **2004**, *7*, 179.
10. Siciliano, T.; Tepore, A.; Micocci, G.; Genga, A.; Siciliano, M.; Filippo, E. *Sens. Actuators. B* **2009**, *138*, 207.
11. Huriet, A.; Daniele, S.; Hubert-Pfalzgraf, L. G. *Mater. Lett.* **2005**, *59*, 2379.
12. Liu, Z.; Yamazaki, T.; Shen, Y.; Kikuta, T. *Appl. Phys. Lett.* **2007**, *90*, 173119.
13. Lin, Y.-H.; Huang, M.-W.; Liu, C.-K.; Chen, J.-R.; Wu, J.-M.; Shih, H. C. *J. Electrochem. Soc.* **2009**, *156*, K196.
14. Ramgir, N. S.; Mulla, I. S.; Vijayamohanan, K. P. *Sens. Actuators B* **2005**, *107*, 708.
15. Wan, Q.; Wang, T. H. *Chem. Commun.* **2005**, 3841.
16. Kolmakov, A.; Klenov, D. O.; Lilach, Y.; Stemmer, S.; Moskovits, M. *Nano Lett.* **2005**, *5*, 667.
17. Kuang, Q.; Lao, C. S.; Li, Z.; Liu, Y. Z.; Xie, Z. X.; Zheng, L. S.; Wang, Z. L. *J. Phys. Chem. C* **2008**, *112*, 11539.
18. Wright, J. S.; Lim, W.; Gila, B. P.; Pearton, S. J.; Johnson, J. L.; Ural, A.; Ren, F. *Sens. Actuators B* **2009**, *140*, 196.
19. Xue, X.; Xing, L.; Chen, Y.; Shi, S.; Wang, Y.; Wang, T. *J. Phys. Chem. C* **2008**, *112*, 12157.
20. Chen, Y.-J.; Zhu, C.-L.; Wang, L.-J.; Cao, P.; Cao, M.-S.; Shi, X.-L. *Nanotechnology* **2009**, *20*, 045502.
21. Park, J. Y.; Choi, S. W.; Lee, J. W.; Lee, C.; Kim, S. S. *J. Am. Ceram. Soc.* **2009**, *92*, 2551.
22. Oh, E.; Choi, H.-Y.; Jung, S.-H.; Cho, S.; Kim, J. C.; Lee, K.-H.; Kang, S.-W.; Kim, J.; Yun, J.-Y.; Jeong, S.-H. *Sens. Actuators B* **2009**, *141*, 239.
23. Kaur, J.; Kumar, R.; Bhatnagar, M. C. *Sens. Actuators B* **2007**, *126*, 478.
24. Vomiero, A.; Bianchi, S.; Comini, E.; Faglia, G.; Ferroni, M.; Sberveglieri, G. *Cryst. Growth Des.* **2007**, *7*, 2500.
25. Liu, Z.; Miyauchi, M.; Yamazaki, T.; Shen, T. *Sens. Actuators B* **2009**, *140*, 514.
26. Choi, S.-W.; Park, J. Y.; Kim, S. S. *Nanotechnology* **2009**, *20*, 465603.
27. Kolmakov, A.; Klenov, D. O.; Lilach, Y.; Stemmer, S.; Moskovits, M. *Nano Lett.* **2005**, *5*, 667.
28. Liu, Z.; Yamazaki, T.; Shen, Y.; Kikuta, T. *Appl. Phys. Lett.* **2007**, *90*, 173119.
29. Fryberger, T. B.; Semancik, S. *Sens. Actuators B* **1990**, *2*, 305.
30. Gao, T.; Wang, T. H. *Appl. Phys. A: Mater. Sci. Process* **2005**, *80*, 1451.